Research Square

Preprints are preliminary reports that have not undergone peer review.
They should not be considered conclusive, used to inform clinical practice,
or referenced by the media as validated information.

Controlling the Droplet Size Distribution of Waste-derived Precipitated CaCO 3 Nanoparticles via Membrane Emulsification of Double Emulsion System Using Porous Organic Polymers

Alireza Bahramian
Hamedan University of Technology
Mohammad Mahdi Salmanipour
bahramian@aut.ac.ir

Hamedan University of Technology

Research Article

Keywords: Calcium carbonate nanoparticles, Industrial Calcium-rich waste, Membrane emulsification, Water-in-oil-in-water emulsion, Porous organic polymer

Posted Date: July 6th, 2026

DOI: https://doi.org/10.21203/rs.3.rs-10019274/v1

License: This work is licensed under a Creative Commons Attribution 4.0 International License.
Read Full License

Additional Declarations: No competing interests reported.

Version of Record: A version of this preprint was published at Brazilian Journal of Chemical Engineering on October 22nd, 2026. See the published version at https://doi.org/10.1007/s43153-026-00728-7.

Controlling the Droplet Size Distribution of Waste-derived Precipitated $CaCO_3$ Nanoparticles via Membrane Emulsification of Double Emulsion System Using Porous Organic Polymers

Alireza Bahramian* and Mohammad Mahdi Salmanipour[1]

Chemical Engineering Department, Hamedan University of Technology, P.O. Box. Hamedan, Iran

Abstract

Size-controllable synthesis of precipitated calcium carbonate (PCC) based on a liquid-liquid process is an important factor influencing the production of nanoparticles (NPs) with uniform particle size. In this study, we present an innovative size-selective method for the synthesis of PCC NPs from industrial calcium-rich waste in a bench-scale unit. The proposed method was based on the membrane emulsification technique by producing double emulsions (DEs) with optimized droplet size distribution. A novel membrane, involving a porous organic polymer functionalized with a hybrid of polyurethane-melamine and polyether(sulfone), was developed as the separation layer. The droplet size distribution of the DEs were analyzed using droplet light scattering. The effects of the internal aqueous phase to organic phase (W1/O) volume ratio, as well as the concentrations of Ca^{2+} and non-ionic surfactants (Span 80 and Tween 80), on the droplet size of DEs were studied before and after filtration. A highly stable DE was achieved by obtaining the lowest mean droplet size and narrow size distribution under optimized conditions (W1/O ratio: 8:1, Ca^{2+} 1.2 M, and surfactant concentration: 1.2 mM). The porous nature of the hydrophobic membrane provides a uniform size distribution of droplets, which represents the suitable antifouling properties. The highest permeate flux and filtration efficiency were attained at W1/O ratios of 12:1 and 8:1, respectively. The proposed membrane showed acceptable reusability, with 95% recovery of refractive flux over three three-cycle cleanings. The good membrane's performance is attributed to the presence of grid-like fibrous hollow spindle structures, which led to the formation of the nanopores/nanochannels.

Keywords: *Calcium carbonate nanoparticles, Industrial Calcium-rich waste, Membrane emulsification, Water-in-oil-in-water emulsion, Porous organic polymer*

* Corresponding author: *bahramian@hut.ac.ir*

1. Introduction

Precipitated calcium carbonate (PCC) powder is widely used in various applications, including papermaking, paint, sealants, and adhesives, serving as a filler, whitener, and softening agent. It is also utilized in food and pharmaceuticals as an additive and neutralizing agent due to its cost-effectiveness, safety, accessibility, and biocompatibility (Krishna Pai and Pillai 2008; Boyjoo et al. 2014; Fadia et al. 2021; Guo et al. 2021). The physicochemical properties of PCC—such as mean particle size and distribution, crystal shape, oil absorption capacity, hydrophilicity, and dispersibility—vary depending on the intended application (Rauscher et al. 2005; Biradar et al. 2011; Jin et al. 2022). PCC nanoparticles (NPs) exhibit promising characteristics, including a high specific surface area and excellent surface activity (Casanova and Higuita 2009; Tang et al. 2025).

The liquid-liquid process based on the Solvay method is known as a main route in industrial production of PCC, in which aqueous solutions containing calcium chloride and sodium carbonate are completely mixed in a continuously operating reactor (Czaplicka N and Konopacka-Łyskawa 2020). Over the past two decades, the industrial production of PCC from calcium-rich waste (CRW) with a high calcium content (22–28 wt%), which would otherwise pose disposal challenges and costs, has become an important research focus (Czaplicka N and Konopacka-Łyskawa 2020; Pei et al. 2023; Liu et al. 2024). CRW, known as a hazardous fine powder due to its high alkalinity (pH 12–13) and the presence of heavy metals, is primarily generated from paper sludge and sugar beet processing (Sharma and Simsek 2020; Dhodduraj et al. 2026). In addition, CRW effluent from the Solvay process can be reused as the reaction medium without carrying out a calcium ion extraction step (Czaplicka N and Konopacka-Łyskawa 2020). The development of advanced technologies has helped reduce the harmful emissions associated with CRW, while producing a

cleaner product that can be sold and reused for the manufacture of high-purity PCC (90–99.5 wt%) (Kaewnoo et al. 2026).

The synthesis of PCC NPs by the sol-gel method, despite its significant advantages over emulsification techniques, faces considerable challenges in achieving a narrow size distribution at the nanoscale due to NP agglomeration and limitations in large-scale production (Gupta 2004; Kaewnoo et al. 2026). Single emulsions are thermodynamically unstable systems prone to droplet coalescence, especially when components with partitioning behavior are involved. In contrast, double emulsions (DEs) consist of droplets encapsulating smaller droplets of different phases, forming a polydispersed system that enhances emulsion stability (Zhang et al. 2016; Wang et al. 2026; da Silva et al. 2026). DEs can be classified into water-in-oil-in-water (W/O/W) and oil-in-water-in-oil (O/W/O) systems (Leister and Karbstein 2020; Yegya et al. 2020). The W/O/W system is a complex dispersion structure in which oil droplets are dispersed within an external continuous aqueous phase, with each oil droplet encapsulating inner water droplets, forming a three-phase "water-oil-water" structure (Liu et al. 2025). This structure allows for the simultaneous encapsulation of hydrophilic and lipophilic substances, controlled release of active components, masking of unpleasant flavors, modification of physicochemical surface properties, and reduction of fat content in various applications (Kumar et al. 2022)

Based on the literature review (Keogh et al. 2017), research on the formation of PCC in DE systems remains quite limited. The presence of an oil phase in multiphase flow enhances PCC formation by providing additional heterogeneous nucleation sites at the oil-water interface. In contrast, an increased oil phase content in an oil-in-water emulsion reduces the tendency for surface scaling due to its preferential wetting characteristics (Bukuaghangin et al. 2015). In one study, a series of multiphase water-oil systems were prepared by mixing nanoscale droplets

containing Ca^{2+} and CO_3^{2-} ions in the presence of a surfactant-stabilized microemulsion to obtain O/W emulsions for the formation of PCC NPs and micellar aggregation (Stawski et al. 2018). Another study highlighted the effect of the cationic surfactant cetyltrimethylammonium bromide on the scale growth rate of PCC NPs. The interfacial interactions caused by surfactant depletion at the water-oil interface slowed the scale growth rate, reduced crystal size, and destabilized the emulsion within a few hours. However, to the best of our knowledge, no comprehensive study has explored the relationship between W/O/W emulsion properties and PCC NPs. Therefore, developing a stable W/O/W emulsion capable of producing uniform PCC NPs remains a significant challenge.

Traditional methods for treating emulsions, such as chemical separation, adsorption, and electrocoagulation, have been widely used; however, they often encounter challenges like high operational costs and difficulties in effectively separating stable emulsions (Zhang et al. 2022; Yeh et al. 2023). In contrast, membrane filtration offers high separation efficiency, ease of operation, environmental friendliness, and cost-effectiveness. It is recognized for its operational simplicity and economic advantages over conventional techniques (Yeh et al. 2023). The hydrophobic nature of many traditional membranes promotes the accumulation of oil droplets within their pores, reducing filtration efficiency due to membrane fouling. To improve the separation of oil-in-water emulsions, it is essential to develop membranes with properties that resist oil fouling. Therefore, modifying membrane surfaces to achieve superhydrophilicity is crucial, as this can prevent oil adhesion and significantly reduce fouling.

The membrane emulsification system is a two-step process that begins with the formation of a droplet on the membrane surface and ends with its detachment from the membrane (Zhang et al. 2022). This method involves pumping the dispersed phase under pressure through a microporous

membrane into the continuous phase, enabling the production of DE systems with narrow droplet size distribution and high monodispersity (Yeh et al. 2023). However, fundamental studies on the use of membrane emulsification for size-selective permeation of droplets in multiphase systems remain limited (Matos et al. 2015; Gehrmann and Bunjes 2017; Ferdowsi et al. 2025). Matos et al. (2015) reported that the membrane emulsification method can generate monodisperse droplets of about 60 μm, which improved the encapsulation efficiency of the DE system. Gehrmann and Bunjes (2017) found that the smallest droplets are obtained by reducing membrane pore size combined with an optimal surfactant concentration. Based on these findings, selecting a suitable membrane with appropriate pore sizes is critical in the emulsification method to achieve the desired droplet size and distribution in DE systems.

Recently, a new class of nanoscale materials known as porous organic polymers (POPs) has attracted significant interest in membrane separation systems due to their exceptional porosity, surface wetting properties, selective permeability, and chemical stability (Bahramian et al. 2025). POP-based thin films have also showed promising results in the separation of organic molecules and inorganic salts, owing to their structural integrity and high specific surface area. These characteristics make them highly promising materials for membrane filtration processes. To the best of our knowledge, the application of POP-based membranes for the size-selective separation of the DE system during the formation of PCC NPs has not yet been investigated at the bench scale.

In this study, we present a novel method for controllable synthesis of PCC NPs in the liquid-liquid process based on Solvay method using a membrane emulsification system with a hydrophobic porous POP-based membrane composed of hybrid polyurethane-melamine (PUMA). First, a high-purity calcium (Ca^{2+})-containing emulsion was synthesized from industrial CRW in

a bench-scale precipitation unit by forming a stabilized DE system. Next, we investigated the effects of the internal aqueous phase to organic phase (W1/O) volume ratio, Ca^{2+} concentration, and surfactant concentration on the droplet size distribution of the DE system before and after filtration through the proposed membrane. Droplet size, number, and size distribution of the DE system were analyzed using droplet light scattering techniques. The size characteristics of the PCC NPs were examined by field emission scanning electron microscopy (FE-SEM) and transmission electron microscopy (TEM). The pore size distribution of the proposed membrane was characterized using a capillary flow porometer. The results were compared to evaluate the impact of the proposed membrane on controlling droplet size distribution of the DE system at various oil/water interfaces.

2. Experimental procedure

2.1. Materials

The main chemical reagents, including sodium carbonate (Na_2CO_3, >99%), sodium hydroxide (NaOH, >97%), hydrochloric acid (HCl, 37%), sodium chloride (NaCl, 99.0%), and ethylenediaminetetraacetic acid (EDTA), were supplied by Merck, Germany. Span 80 ($C_{24}H_{44}O_6$, >99%), Tween 80 (Polysorbate 80, $C_{64}H_{124}O_{26}$, >99%), ammonia (25%), and ethanol (EtOH, 99.8%) were supplied by Sigma-Aldrich, USA. Paraffin oil with a transparent appearance (USP Grade) was purchased from Sarvestandarou, Iran. Deionized (DI) water was obtained from an ultrapure water system (Mili-Q, Merck-Milipore, 10). Lime sludge waste, used as a CRW sample, was collected from the effluent landfill of the Hegmatan Sugar Factory, Hamedan, Iran. The CRW powder was initially calcined at 1000 ºC to remove organic impurities and ensure complete conversion of lime to calcium oxide (CaO). Subsequently, the CaO was mechanically crushed and ground using a ball mill to produce a fine powder.

2.2. Synthesis of PCC NPs

2.2.1 Preparation of Calcium enriched slurry

The prepared CaO fine powder was poured into the first continuous stirred tank reactor (CSTR-1) to react with DI water under mild stirring. Fumed HCl was added dropwise into the CSTR to form a hydrated lime solution. The dilution ratio (CaO to DI water) was set at 1:8. The hydrated lime solution was gradually converted to a calcium hydroxide solution by stirring at 400 rpm for 30 min. The effluent from CSTR-1 was directly transferred to the first mixing tank. A chelating agent (EDTA) and ammonia was added dropwise to the vessel. Additionally, 0.1 M NaCl was added to the reactor to maintain the desired pH. Finally, the contents of the mixing vessel were pumped into the CSTR-2 reactor for the conversion of the $Ca(OH)_2$ solution into $CaCl_2$ solution. The $CaCl_2$ slurry was then transferred to a second mixing vessel using a BT400-2 J peristaltic pump (220 V, 600 mA, Baoding Longer Pump Co., Ltd.). The pumps were calibrated before each run to ensure the correct flow rate of the Ca-enriched slurry.

2.2.2 Preparation of DE system

The synthesis of PCC NPs was followed by the dispersion of the primary emulsion—comprising a dispersed phase (aqueous phase) and a dispersing medium (oil phase)—into a second mixing vessel to form a stable DE system. The details of the procedure are described as follows: In the first step, the internal aqueous phase containing a CaCl2 slurry with varying Ca^{2+} concentrations (0.6, 0.8, 1.0, 1.2, 1.4, and 1.6 M) and a mixture of Span 80 and paraffin oil were combined at different W1/O volume ratios (2:1, 4:1, 6:1, 8:1, 10:1, and 12:1) in the first vessel. This mixture was subjected to vigorous mixing at 6,000 rpm for 10 minutes to form a W1/O emulsion. In the second step, an external aqueous phase (W2), containing a mixture of sodium carbonate solution and varying concentrations of Tween 80, was prepared in a second vessel under

vigorous mixing at 6,000 rpm for 10 minutes. Finally, the contaminant from the first vessel was slowly added to the second vessel while mixing at 3,000 rpm, followed by further homogenization at 6,000 rpm for 3 minutes. The formation of PCC NPs was occurred through the reaction of Ca^{2+} and CO_3^{2-} ions within the W1/O/W2 emulsion droplets, with the Ca^{2+}/CO_3^{2-} molar ratio adjusted according to the stoichiometry of the chemical reaction. After 10 minutes of mixing at 6,000 rpm using a high-speed homogenizer, CO_3^{2-} ions in the external phase were transported across the emulsion droplets to react with the Ca^{2+} ions in the internal phase.

Well-stabilized DE systems are typically obtained at stirring speeds between 3000 and 6000 rpm, which provide sufficient mechanical energy to produce small droplets. However, excessively high stirring speeds may cause droplet coalescence by increasing droplet velocity and collision rates. Additionally, a high homogenizer stirring speed can increase the emulsion viscosity, resulting from a decrease in the droplet size of the dispersed oil phase (De Hert and Rodgers 2017). Based on a literature review, an optimized stirring speed of 6,000 rpm and a stirring time of 10 minutes were selected for the measurements to maximize the droplet breakage rate.

PCC NPs are typically formed within emulsion droplets and subsequently transferred to a POP-based membrane for further filtration and purification. The formation of PCC NPs is followed by centrifugation and solvent evaporation from the dispersed phase. Scheme 1 illustrates a schematic representation of PCC NPs preparation through the formation of DE system. Two non-ionic surfactants, Span 80 and Tween 80, were selected based on their hydrophilic-lipophilic balance (HLB) values, as reported in the literature (Ghasemi et al. 2020). Tween 80 (HLB ~15) is highly hydrophilic and ideal for stabilizing O/W emulsions, whereas Span 80 (HLB ~4.3) is more lipophilic and suitable for W/O emulsions (Márquez et al. 2010). The concentrations of both

emulsifiers were varied from 0.6 to 1.6 mM. The concentrations of Ca^{2+} and CO_3^{2-} ions were determined according to the literature (Somani et al. 2006).

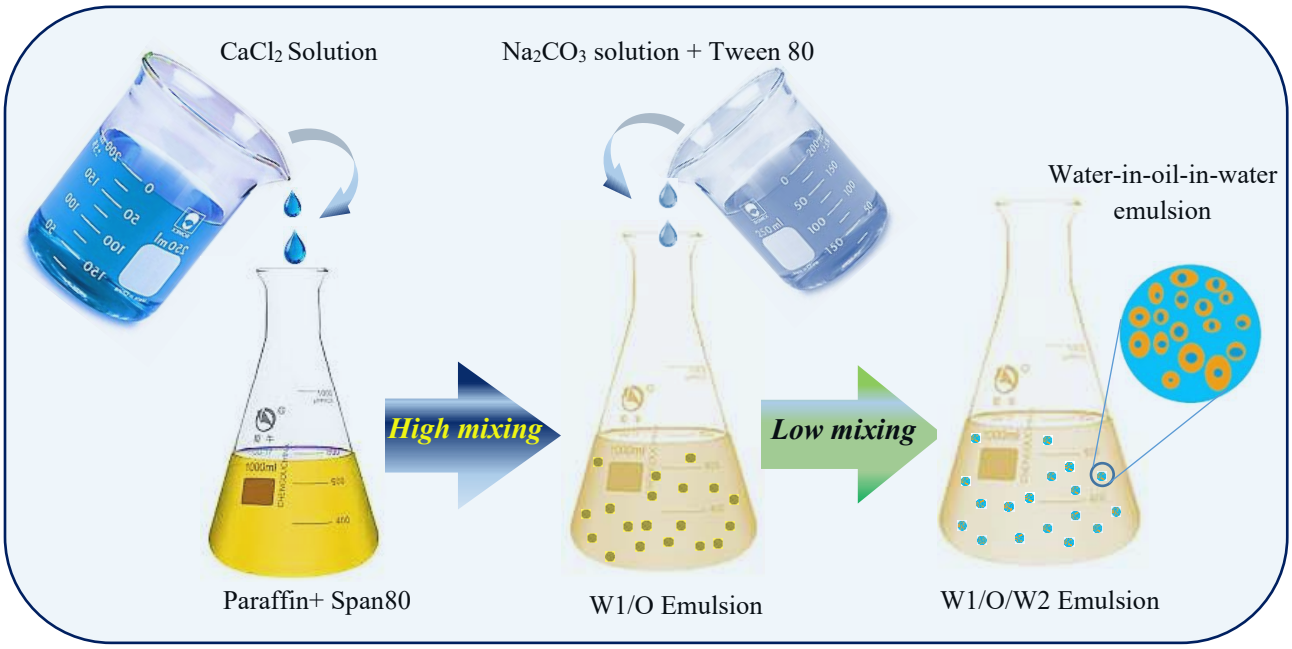

Scheme 1. Schematic image of PCC NPs preparation through formation of DE.

2.3.3. Fabrication of POP-based membrane

Figure 1 presents the internal views of the electrospinning device (Nano Azma Company, Iran). The system consists of two plastic syringes with sharpened nozzles for rapid spraying of the polymeric solution onto a rotating aluminum collector plate, which is used to fabricate the POP-based membrane. The rotating plate is positioned horizontally relative to the nozzle tips. The electric field strength is provided by a high-intensity power supply. Polyether sulfone (PES) was used to stabilize the polymeric solution. Consequently, PUMA (4.7 wt%) was blended with the PES matrix. The resulting polymeric solution was directly injected through a metallic nozzle onto a rotating aluminum plate. The rotating plate was positioned 15 cm from the nozzle tip to deposit the synthesized polymeric solution onto its surface, forming a thin-film membrane with the desired thickness. An electric field of 18 kV/cm was applied to spray the polymeric solution onto the

collector metal plate (Fig. 1). The device operation was controlled by adjusting the voltage at a fixed distance while varying the volumetric injection rate of the solution (2 mL/h).

Figure 1. The electrospinning apparatus components [1: rotating plate, 2: Injector, 3: adjustable rotating plate, 4: magnetic field, 5: holder, 6: fiber container].

2.4. Analysis and characterization

2.4.1. DE system

The droplet size distribution of the DE system, both before and after filtration through the POP-based membrane, were measured using dynamic light scattering (DLS; HORIBA Scientific, SZ-100-S2). Measurements were performed on a series of DE systems with mean relative refractive indices of 1.470 (paraffin oil) and 1.333 (DI water), and a mean absorbance value of 0.01. To minimize multiple scattering effects, the emulsions were diluted to a final droplet concentration of 0.005 wt.% prior to testing, following a 120-second equilibration period. Each sample underwent multiple readings, and the resulting data were processed and analyzed using the Smoluchowski model (von Smoluchowski 1921).

Micromorphological observations of the DE system were conducted using an optical microscope (BX53, Olympus Optical Co., Ltd., Tokyo, Japan) equipped with a CCD camera

(Olympus Optical Co., Ltd., Tokyo). A single droplet of the diluted emulsion was placed on a microscope slide and covered with a coverslip for observation at 40× magnification. The resulting images were analyzed using ImageJ software (ImageJ 1.52p). The mean droplet size was determined using the volume-weighted mean diameter (D_{43}) and the surface-weighted mean diameter (Sauter diameter, D_{32}), calculated as follows:

$$D_{43} = \frac{\sum n_i d_i^4}{\sum n_i d_i^3} \quad (1)$$

$$D_{32} = \frac{\sum n_i d_i^3}{\sum n_i d_i^2} \quad (2)$$

where n_i is the number of droplets of diameter d_i (Chouaibi et al. 2019).

2.4.2. PCC NPs and POP-based membrane

The morphological structure of the PCC NPs and POP-based membrane was examined using FE-SEM analysis (FEI QUANTA 200) equipped with an EDS analyzer (EDAX Silicon Drift 2017). The size of the PCC NPs was determined by TEM analysis (JEM-2100F). The crystal structure of the PCC powder was characterized using a Philips PW 1710 diffractometer with Cu Kα radiation (λ = 1.54056 Å). The crystal structure of the resulting PCC NPs was studied by XRD over a 2θ range of 20° to 80°, with a step size of 0.04°. The pore size distribution of the POP-based membrane was characterized using a capillary flow porometer (Porometer 3G zh, Quantachrome Instruments).

2.4.3. Evaluation of membrane performance

Figure 2 shows the filtration unit based on the RO process and its accessories, which consist of a stirred vessel, a feed solution supply pipe, a peristaltic pump, a cylindrical steel vessel, a thin-film membrane, and a permeate solution collection container. When pressure (typically between 0.5 bar and 20 bar) is applied to the filtration system, the feed solution is continuously stirred and passed through the membrane cell.

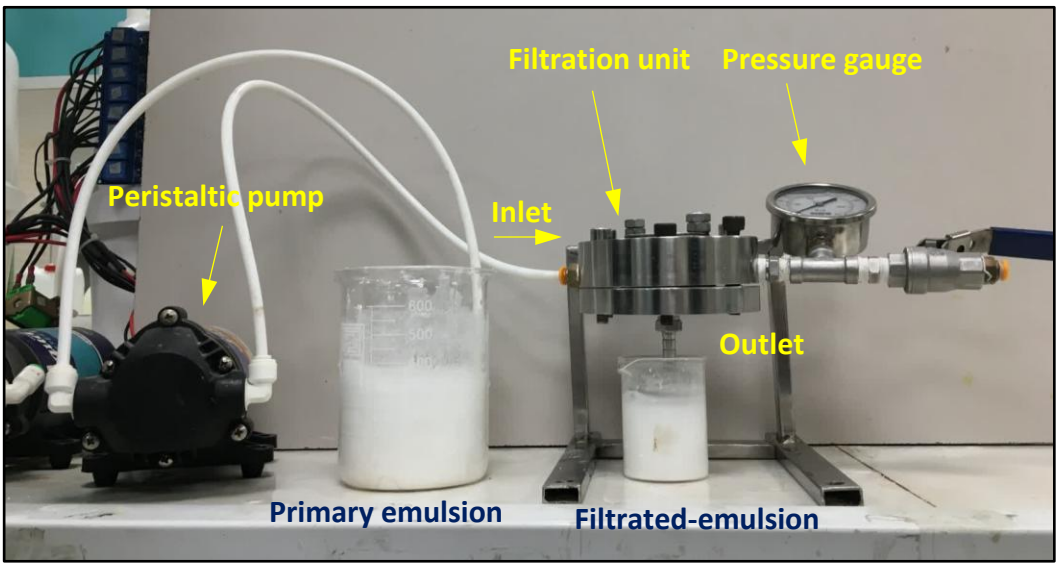

Figure 2. The image of filtration unit based on RO process and its accessories.

The permeate flux of oil phase (J_o, L.m^{-2}.h^{-1}) was determined by the following equation:

$$J_o = \frac{V}{A \times \Delta t} \quad (3)$$

where V is the volume of permeated oil (L), A represents the effective membrane area (m^2), and Δt is the permeation time (h).

The separation efficiency (E) of the prepared membranes was determined according to the following equation:

$$E = \left(1 - \frac{C_1}{C_0}\right) \times 100\% \quad (4)$$

where C_0 and C_1 are the water concentration before and after the separation process, respectively.

The fouling resistance evaluation of the POP-based membrane was evaluated at different W1/O volume ratios of the primary emulsions. Fouling experiments were carried out for 120 min, until the total volume of permeate emulsions was collected in a container.

3. Results and discussion

3.1. Membrane characterization

Figure 3 shows the FE-SEM image of the surface, (b) low-magnification, and (c) high-magnification cross-sectional images, (d) surface pore size distribution, and (e) EDS analysis of the POP-based membrane. The inhomogeneity observed on the surface of the POP-based membrane, caused by the presence of nanopores, is quantitatively revealed by the FE-SEM image (Fig. 3a). This inhomogeneity is attributed to the incorporation of porous PUMA (4.7 wt%) within the pristine PES framework. The PUMA structure adheres to the PES matrix, forming an agglomerated structure that is firmly embedded with some crack deflections. Smaller cracks exhibit a lower rupture ratio compared to larger cracks (less than 200 μm). The presence of nanopores facilitates effective pathways within the membrane structure, which can reduce the transfer resistance of the emulsion caused by capillary suction (Hailan et al. 2021).

The outline of the film thickness is indicated by a dotted line in the low-magnification cross-sectional view of the membrane matrix (Fig. 3b). The proposed membrane has an average thickness of 200.2 ± 30.2 μm. A high variation in the measurement of film thickness, caused by significant surface inhomogeneity, resulted in considerable surface roughness of the membrane. A pore size gradient along the membrane thickness, characterized by distinct sandwich-like layers, was observed in the high-magnification cross-sectional image (Fig. 3c). Notably, grid-like fibrous spindle structures with diameters of 10–20 nm and lengths of a few microns (~1–3 μm) were quantitatively observed in the corresponding image, which is attributed to the presence of POP structures on the film surface.

Furthermore, since sieving is essential in membrane separation to ensure effective filtration performance, large droplets are expected to be removed by the small pores of the fibrous spindle

structure, thereby enhancing emulsion filtration. The proposed membrane exhibits a wide pore diameter range of 16–268 nm. The formation of hollow fiber nanopores and nanochannels in the prepared membrane enables it to achieve a high rejection capacity for emulsion droplets larger than the membrane's pore sizes (Fig. 3d). EDS analysis confirmed that the membrane composition is a mixture of PES and PU, containing carbon (71.3 wt%), oxygen (11.57 wt%), nitrogen (5.24 wt%), and sulfur (11.88 wt%).

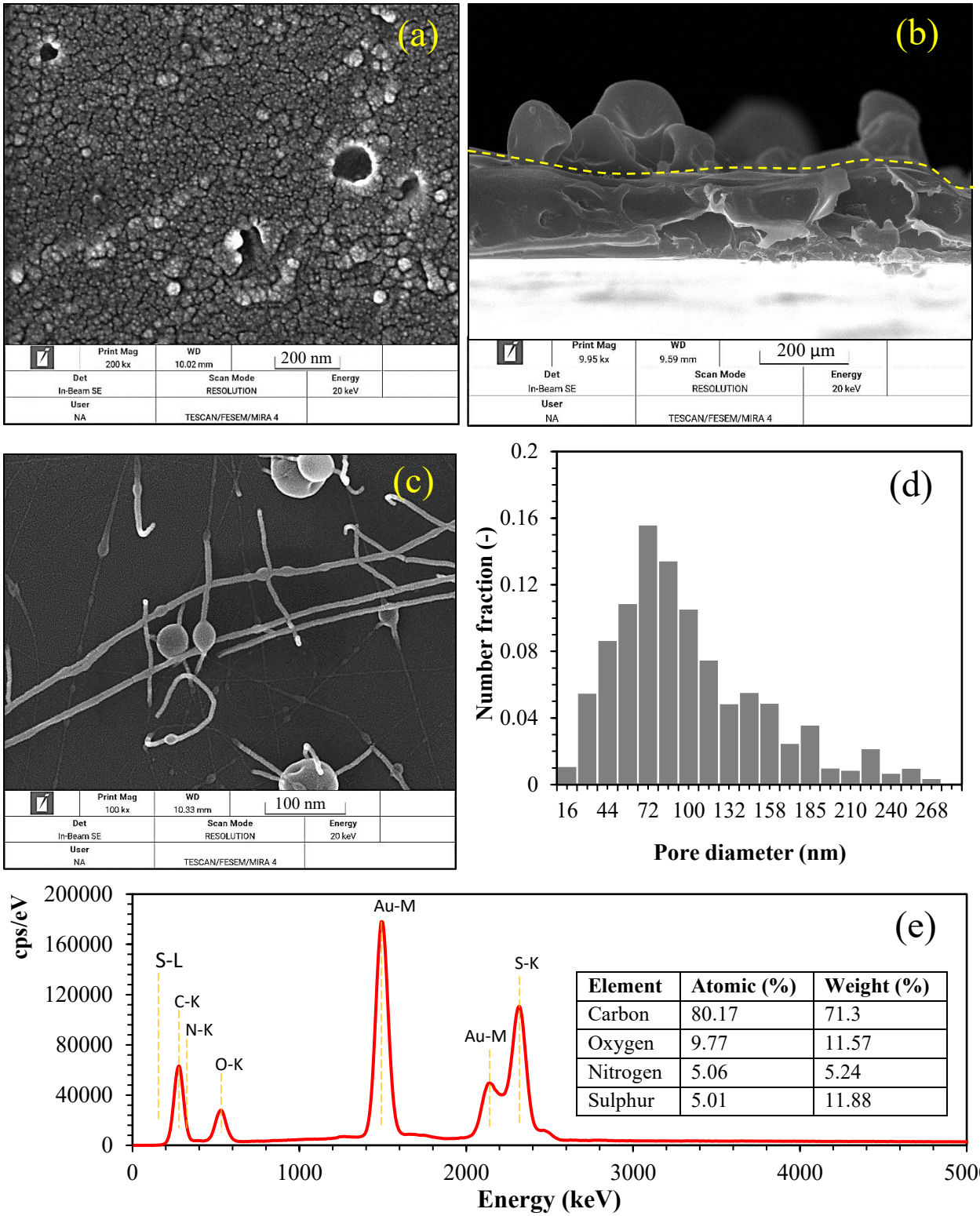

Element	Atomic (%)	Weight (%)
Carbon	80.17	71.3
Oxygen	9.77	11.57
Nitrogen	5.06	5.24
Sulphur	5.01	11.88

Figure 3. Characterization of the POP-based membrane (a) FE-SEM image of surface, (b) low-magnification and (c) high-magnification cross-sectional images, (d) pore size distribution, and (e) EDS analysis and weight percentage of corresponding atoms.

3.2. Droplet size distribution of DE before filtration

Figure 4 presents the optical micrograph and the corresponding droplet size distribution curve of the DE system before filtration by the POP-based membrane. The Ca^{2+} concentration was 1.2 M, and the W1/O volume ratio was fixed at 6:1. The concentrations of Span 80 and Tween 80 were maintained at 1.2 mM. The dark regions represent the W1/O emulsion droplets, while the bright areas correspond to the W2 phase, confirming a fine dispersion of internal W1/O phase droplets and the successful formation of the DE system (Reichhardt and Parsek 2019). The optical micrograph also confirmed the presence of Type A DE droplets during coalescence phenomena, representing the simplest system consisting of relatively small droplets with nearly single internal aqueous phase droplets (Florence et al. 1981). The coexistence of lipophilic small-sized droplets and hydrophilic larger droplets in the images indicates the optimal performance of the DE (Li et al. 2021). The DE was characterized as polydisperse, containing a mixture of small and large droplets. The corresponding curve clearly indicates a broad droplet size distribution, extending up to approximately 100 µm, with a mean droplet size of 47.8 µm.

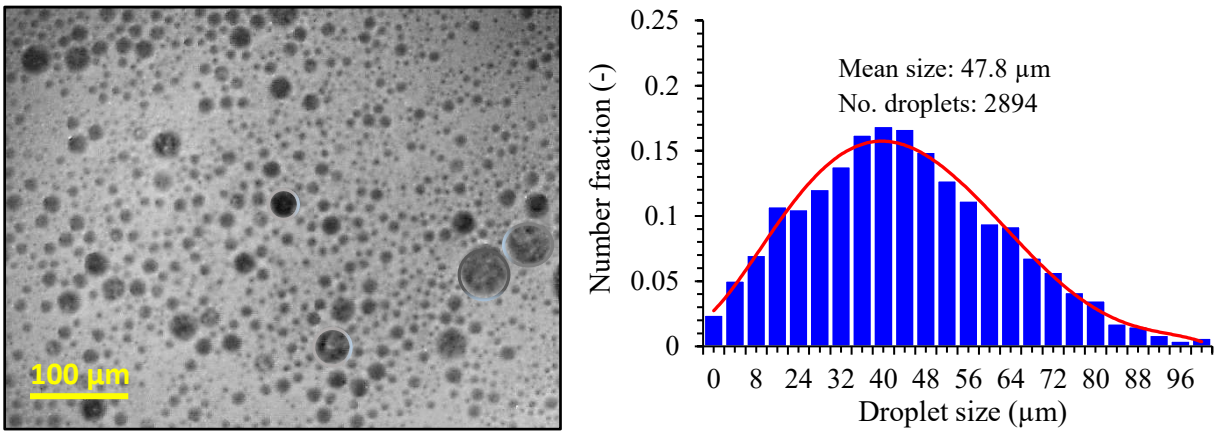

Figure 4. The optical micrograph and corresponding droplet size distribution curve before filtration [Ca^{2+} concentration was 1.4 M, and the W1/O volume ratio was 8:1. The surfactants concentration were fixed at 1.2 mM].

Figure 5 shows the optical micrographs and droplet size distribution curves of the DE prepared at varying Ca^{2+} concentrations. The concentrations of Span 80 and Tween 80 were fixed at 1.2 mM, while the W1/O volume ratio was maintained at 6:1. The results indicate that both the size and number of droplets slightly increased as the Ca^{2+} concentration rose from 0.6 M to 0.8 M, primarily due to coalescence phenomena. An increase in the number of droplets with rising Ca^{2+} concentration suggests a higher rate of nucleation sites and larger primary droplet size, consistent with classical nucleation theory (Al Nasser et al. 2008). Within the Ca^{2+} concentration range of 1.0–1.2 M, the mean size and number of small droplets remained relatively constant, indicating a steady rate of droplet collision and coalescence in the DE.

An increase in the Ca^{2+} concentration from 1.2 to 1.4 M led to a significant increase in both the mean size and number of droplets. Further increasing the Ca^{2+} concentration from 1.4 to 1.6 M resulted in the appearance of large droplets in the micrograph, indicating a high likelihood of droplet collision and coalescence in the DE system. This finding is consistent with previous studies, which suggest that emulsion water droplets can partially overlap, leading to water-water coalescence at high dispersed phase concentrations (Maghamian et al. 2021).

Furthermore, an increase in the dispersed phase concentration led to changes in the physicochemical properties of the DE, resulting in decreased sedimentation (Buyukkestelli and Nehir El 2021). The density and viscosity of the DE system depend on the dispersed phase concentration, where low and high concentrations correspond to Newtonian and non-Newtonian (shear-thinning) fluid behavior, respectively (Pal 2008). Increasing the dispersed phase ratio raises viscosity, which in turn reduces sedimentation [23]. This phenomenon is well explained by Stokes' law, which states that droplet size and the viscosity of the continuous phase directly affect gravitational separation (Akhtar et al. 2007).

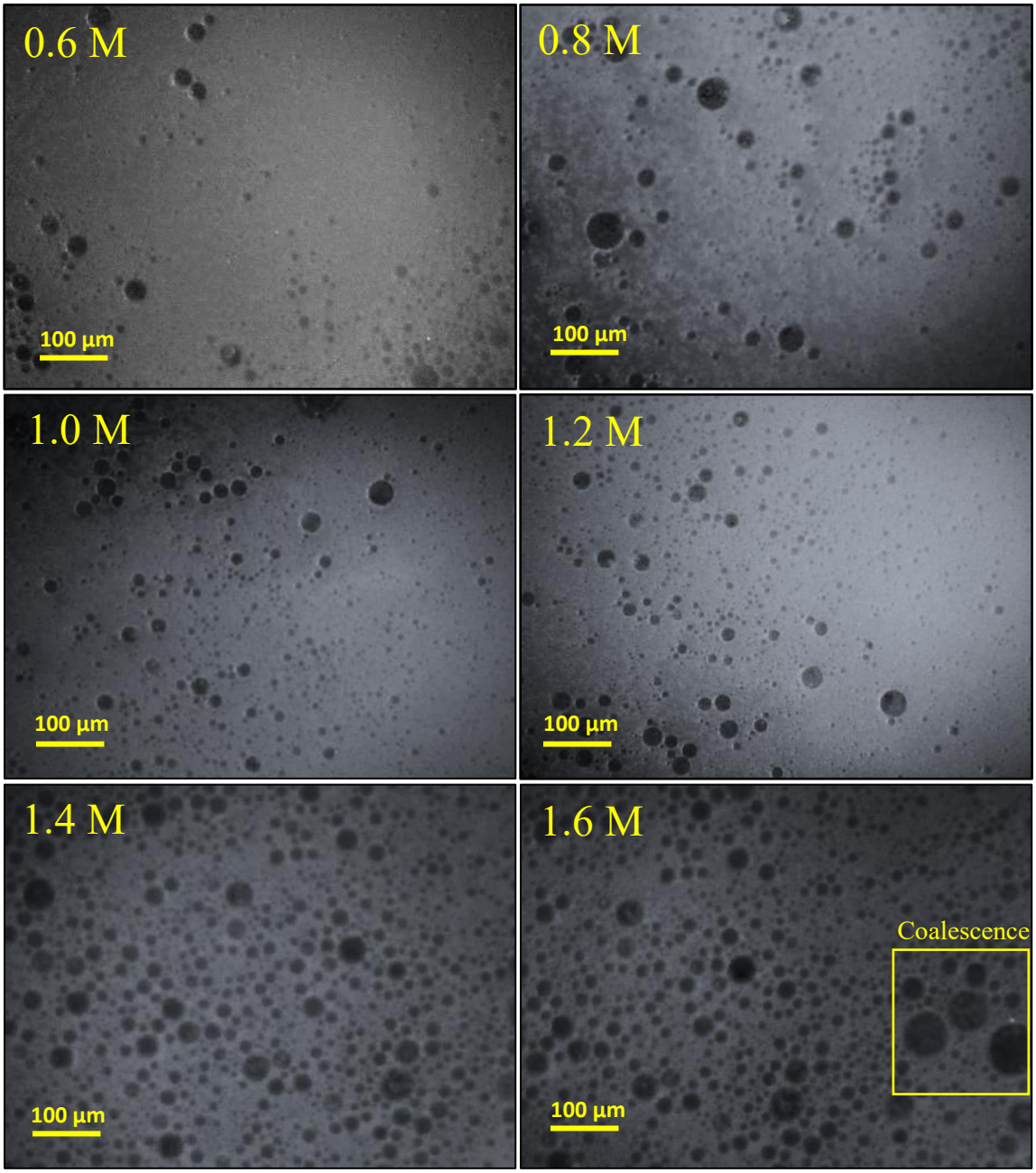

Figure 5. The optical micrographs of DE as-prepared at different Ca^{2+} concentrations [The surfactants concentrations were fixed to be 1.2 mM, and W1/O volume ratio was 6:1].

Figure 6 shows the droplet size distribution of the DE as prepared at various Ca^{2+} concentrations. The W1/O volume ratio of the system was maintained at 8:1, while the concentrations of Span 80 and Tween 80 were fixed at 1.2 mM. The results indicate that the mean

droplet size of the DE increased as the Ca^{2+} concentration rose from 0.6 to 1.6 M. At low Ca^{2+} concentrations, the droplets in the DE system were limited to sizes smaller than 56 μm. An increase in Ca^{2+} concentration from 0.6 to 0.8 M led to an increase in both the mean size and number of droplets, attributed to droplet coalescence phenomena. The mean droplet size remained relatively constant at Ca^{2+} concentrations between 1.0 and 1.2 M, indicating a minor effect of Ca^{2+} concentration on the results.

The results also indicate that the number of droplets followed an opposite trend with increasing Ca^{2+} concentration. In the Ca^{2+} concentration range of 0.6 to 1.0 M, the number of droplets significantly increased to reach its maximum value, then slightly decreased due to droplet coalescence. An increase in Ca^{2+} concentration from 1.2 to 1.4 M led to an increase in droplet size, while the number of droplets decreased. At high dispersed phase concentration (more than 1.4 M), droplet sizes extended up to 100 μm, caused by water-water coalescence phenomena.

A two-way ANOVA results indicate the Ca^{2+} concentration had a statistically significant effect on the droplet size distribution of the DE system (p-value = 0.0361). An increase in the Ca^{2+} concentration from 0.6 to 1.6 M resulted in an average increase of 276.1% in the mean droplet size. A minor change in mean droplet size was observed when the Ca^{2+} concentration increased from 1.0 to 1.2 M. In contrast, a major change in mean droplet size occurred when the Ca^{2+} concentration increased from 1.2 to 1.4 M, which represent the critical Ca^{2+} concentration, indicating that even a slight change in Ca^{2+} concentration in the dilution solution significantly affected the droplet size distribution curve.

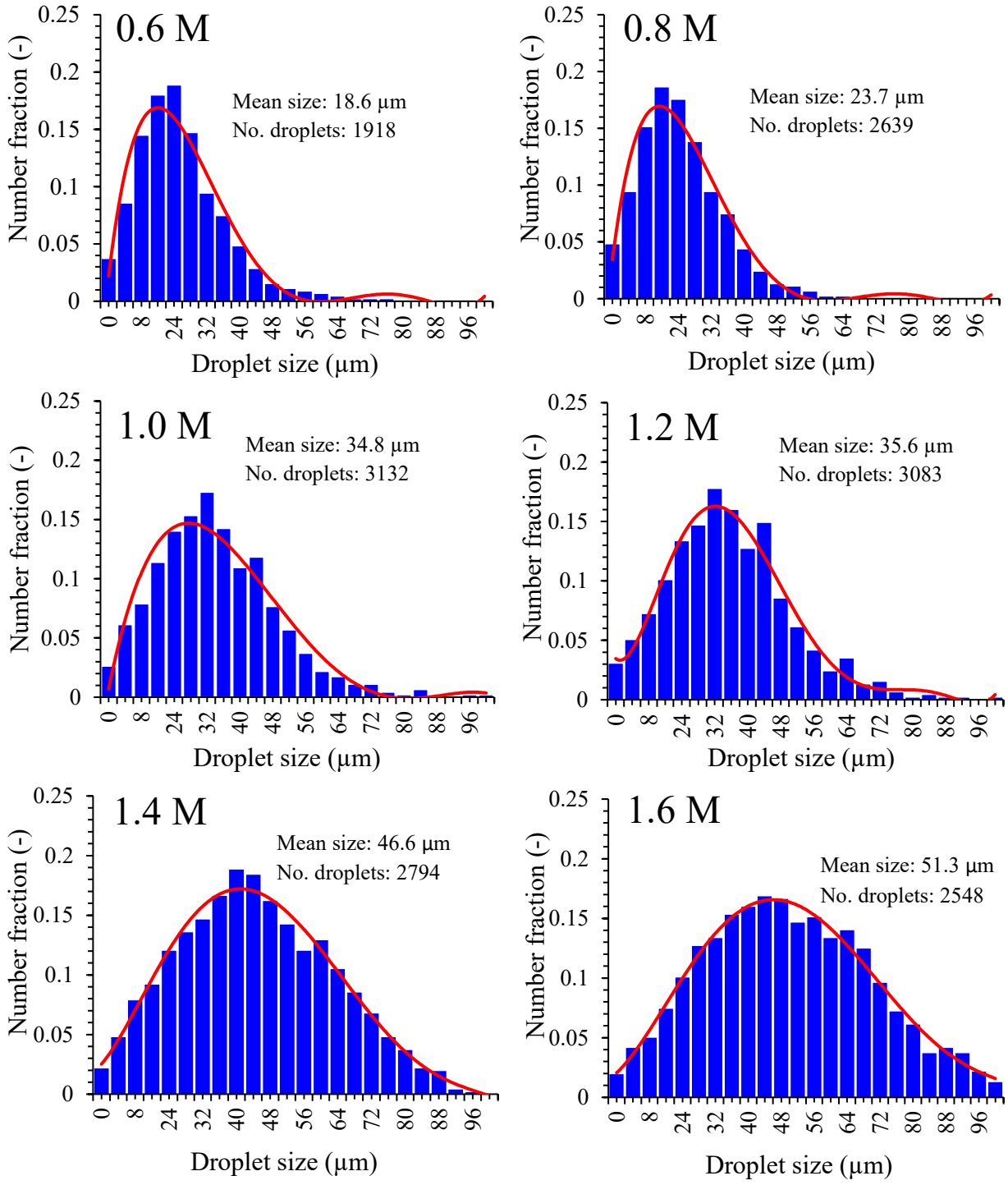

Figure 6. The droplet size distribution of the DE at different Ca^{2+} concentrations [The concentrations of Span 80 and Tween 80 were fixed to be mM, and W1/O volume ratio was 8:1].

Figure 7 shows the droplet size distribution of the DE prepared at different W1/O volume ratios. The concentrations of Ca^{2+} and CO_3^{2-} were 1.2 M and 0.8 M, respectively. The

concentrations of Span 80 and Tween 80 were fixed at 1.2 mM. The results indicate that the droplet size distribution is affected by the W1/O volume ratio. An increase in the W1/O volume ratio from 2:1 to 4:1, and then from 6:1 to 8:1, led to a significant decrease in droplet size—from 54.9 to 48.6 μm, and then from 34.5 to 24.6 μm, respectively. In contrast, an increase in the volume of the dispersed phase from 10:1 to 12:1 caused a slight increase in the mean droplet size, from 25.7 to 27.8 μm, respectively. The droplet size distribution curve of DE as-prepared at W1/O volume ratio of 8:1 and 10:1 was narrower than that at other ratios, indicating the best performance of the DE.

At low W1/O volume ratios of 2:1 and 4:1, a wide size distribution of droplets was obviously observed, where droplet sizes exceeded 70 μm, indicating occurrence of droplet coalescence caused by difference between two dielectric constants of dispersed and continuous phases. Based on Cohen's rule (Kotsuki et al. 2016), in a dispersion system composed of two phases with different dielectric constants, the phase with the higher dielectric constant becomes positively charged, while the other phase becomes negatively charged (Marinova et al. 1996). At a low W1/O volume ratio (2:1), paraffin oil droplets are more dispersed into the aqueous phase during emulsification. Conversely, the viscosity of the W1/O system decreases at low W1/O volume ratios, as the oil droplet size increases due to oil-oil coalescence. Therefore, an increase in the mean droplet size and a decrease in the number of droplets are observed at low W1/O volume ratios. Ostwald ripening phenomena, including the diffusion of smaller droplets into larger ones, occur when the number of dispersed oil droplets becomes too large, leading to growth in oil droplet size and a reduction in the emulsion's viscosity (Yeh et al. 2023).

At a high W1/O volume ratio (12:1), an increase in the volume of the dispersed phase can lead to the coalescence of large water droplets, which in turn causes an increase in droplet size.

Additionally, at high W1/O initial volume ratio, the viscosity of DE increases and the probability of water droplets collision increases, leading water-water coalescence.

In the W1/O volume ratios of 8:1 and 10:1, a minimum mean droplet size and a maximum number of droplets of the DE was observed, indicating optimal emulsion stability. Additionally, the droplet size distribution curves in the above-mentioned range were narrower compared to other W1/O volume ratios, where droplet sizes are not exceeded 60 μm. An increase in the W1/O volume ratio from 10:1 to 12:1 resulted in a significant decrease in the number of droplets. Therefore, the highest degree of emulsification and best oil dispersion performance in the DE was achieved at a W1/O volume ratio of 8:1.

A two-way ANOVA result showed that the significant effect of W1/O volume ratio on the droplet size distribution of the DE in the ratios range of 2:1 to 8:1 (p-value = 0.0224). An increase in the W1/O volume ratio from 2:1 to 8:1 resulted on an average 44.8% decrease in the mean droplet size, indicating W1/O volume ratio significantly affected the droplet size distribution. In contrast, the ANOVA results indicated that the W1/O volume ratio had not affect the droplet size distribution of DE in the ratios range of 8:1 to 12:1 (p-value = 0.1342). A minor change in mean droplet size was observed in the W1/O volume ratios range of 8:1 to 10:1.

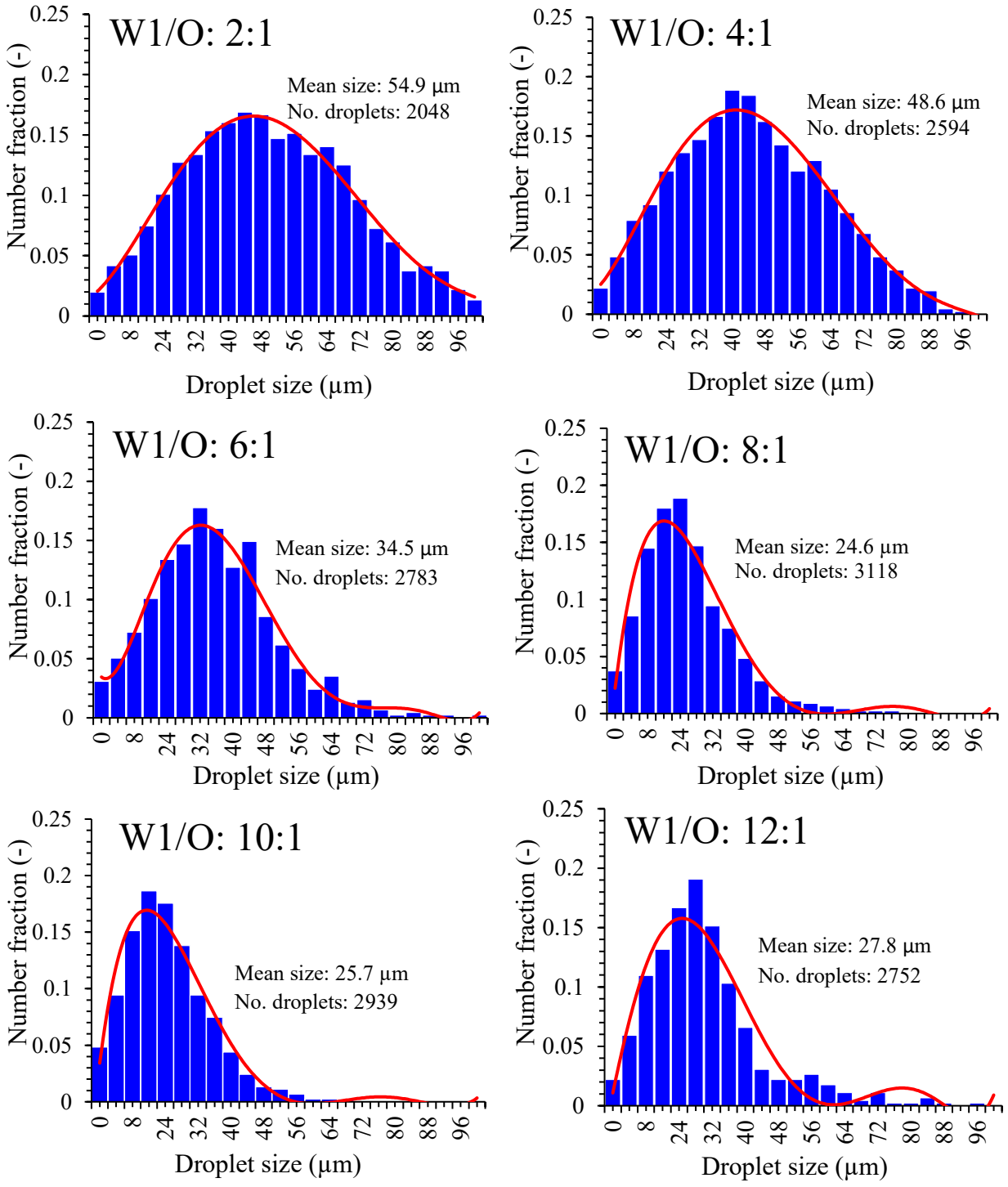

Figure 7. The droplet size distribution of the DE prepared at different W1/O volume ratios, where Ca^{2+} and CO_3^{2-} concentrations were 1.2 and 0.8 M, respectively [The concentrations of Span 80 and Tween 80 were fixed to be 1.2 mM].

Figure 8 shows the droplet size distribution of DE prepared at different Span 80 concentrations (% w/v) in the oil phase, maintaining at a constant W1/O volume ratio of 10:1. The concentrations of Ca^{2+} and CO_3^{2-} were 1.2 M and 0.8 M, respectively. An increase in the Span 80 concentration as non-ionic surfactant from 0.6 to 1.2 mM resulted in a significant reduction in the mean droplet size, enhancing the colloidal stability of the DE. However, a further increase in Span 80 concentration from 1.2 to 1.6 mM negatively affected the mean droplet size, indicating the critical micelle concentration (CMC) point at 1.2 mM. This result was in good agreement with previous study, which reported that the stability of DE was increased by seven days without any droplet coalescence due to the use of Span 80 (Leong et al. 2017). The presence of lipophilic surfactant decreases the surface tension of the oil phase, resulting in the droplet's smaller size and better emulsion stability (Kumar et al. 2025). High concentrations of surfactant agent provide a high surface-to-mass ratio of droplets in the DE system, while the surfactant concentrations cannot exceed the CMC point (1.2 mM) to ensure that acceptable daily intakes are not exceeded (Cox et al. 2020). The droplet flocculation phenomena may have occurred due to a high surfactant concentration, where attractive forces (Van der Waals interactions) between dispersed phase droplets overcome the repulsive forces (electrostatic and short-range interaction) between the continuous phase (Akhtar et al. 2007).

A two-way ANOVA result showed that the Span 80 concentration had a notable effect on the droplet size distribution of the DE system (p-value = 0.0321). An increase in the surfactant concentration from 0.6 to 1.2 mM, resulted on an average 56.6% decrease in the mean droplet size, indicating a significant effect of Span 80 concentration in the mentioned range (p-value = 0.02465). In contrast, the statistical results indicated that the Span 80 concentration had not affect the droplet size distribution after CMC point.

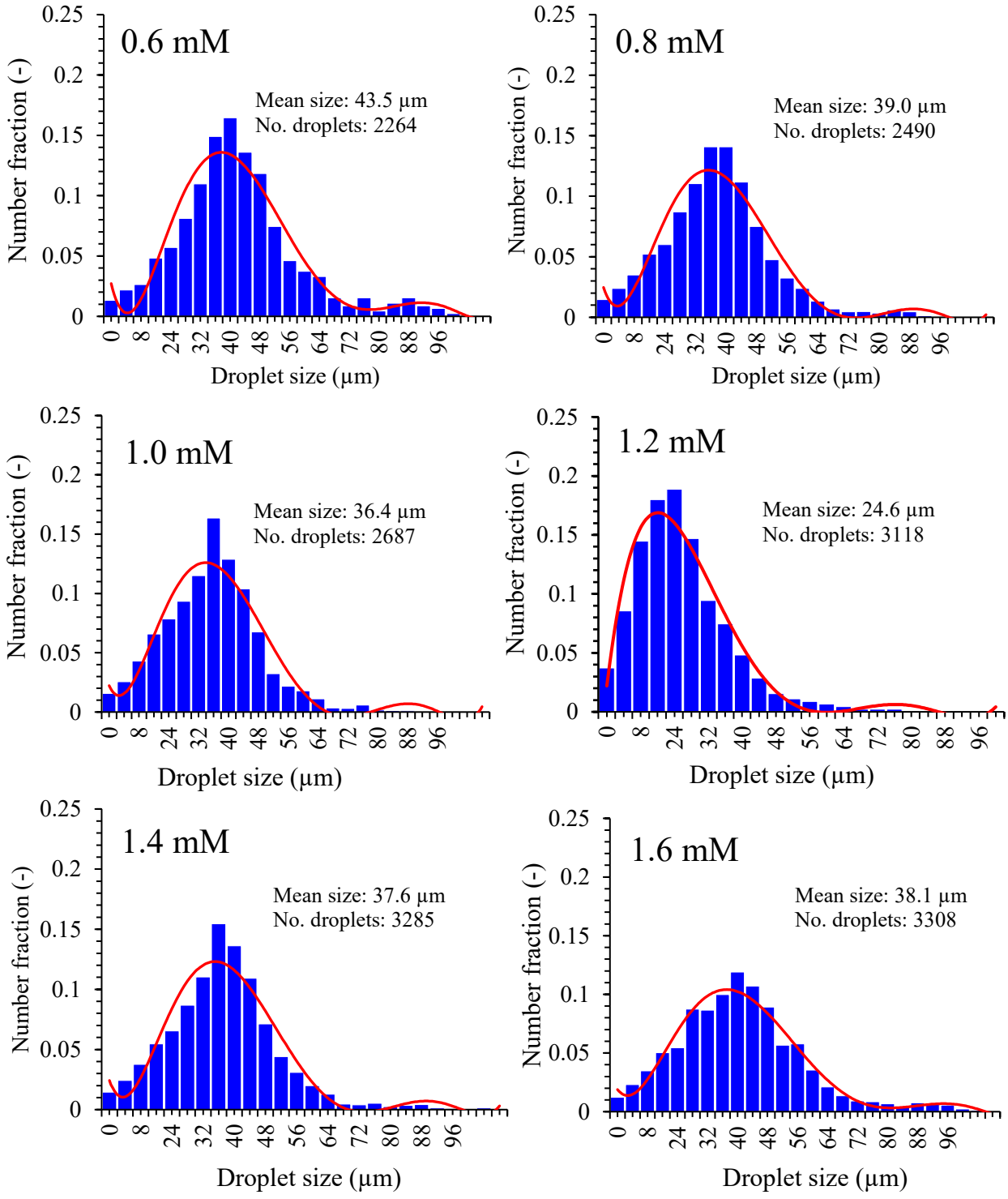

Figure 8. The droplet size distribution of the DE prepared at different Span 80 concentrations [The W1/O volume ratio was 8:1, while Ca^{2+} and CO_3^{2-} concentrations were 1.2 and 0.8 M, respectively].

Figure 9 shows the droplet size distribution of the DE prepared at different Tween 80 concentrations in the aqueous phase at W1/O volume ratio of 8:1, where Ca^{2+} and CO_3^{2-} concentrations were 1.2 and 0.8 M, respectively. The results indicated that the mean size of droplets in the DE system was decreased with an increase in the concentration of Tween 80 from 0.6 to 1.2 mM. At Tween 80 concentration of 1.2 mM, the droplet size distribution was narrower than that of the other concentrations. An additional increase or decrease in the Tween 80 concentration from 1.2 to 1.6 mM or 1.2 to 0.6 mM, respectively, led to a significant change in the droplet size distribution of the DE, which indicates 1.2 mM is a CMC point. An increase in the Tween 80 concentration to reach the CMC point led to the formation of a narrow droplet size distribution. This result confirmed that the Tween 80 concentration plays a vital role in the mean droplet size and size distribution of DE.

A two-way ANOVA result showed that the Tween 80 concentration had a notable effect on the droplet size distribution of the DE system (p-value = 0.0349). An increase in the Tween 80 concentration from 0.6 to 1.2 mM resulted in, on average, a 47.8% decrease in the mean droplet size. However, the statistical results indicated that the low and high concentrations of Tween 80 had not affected the droplet size distribution.

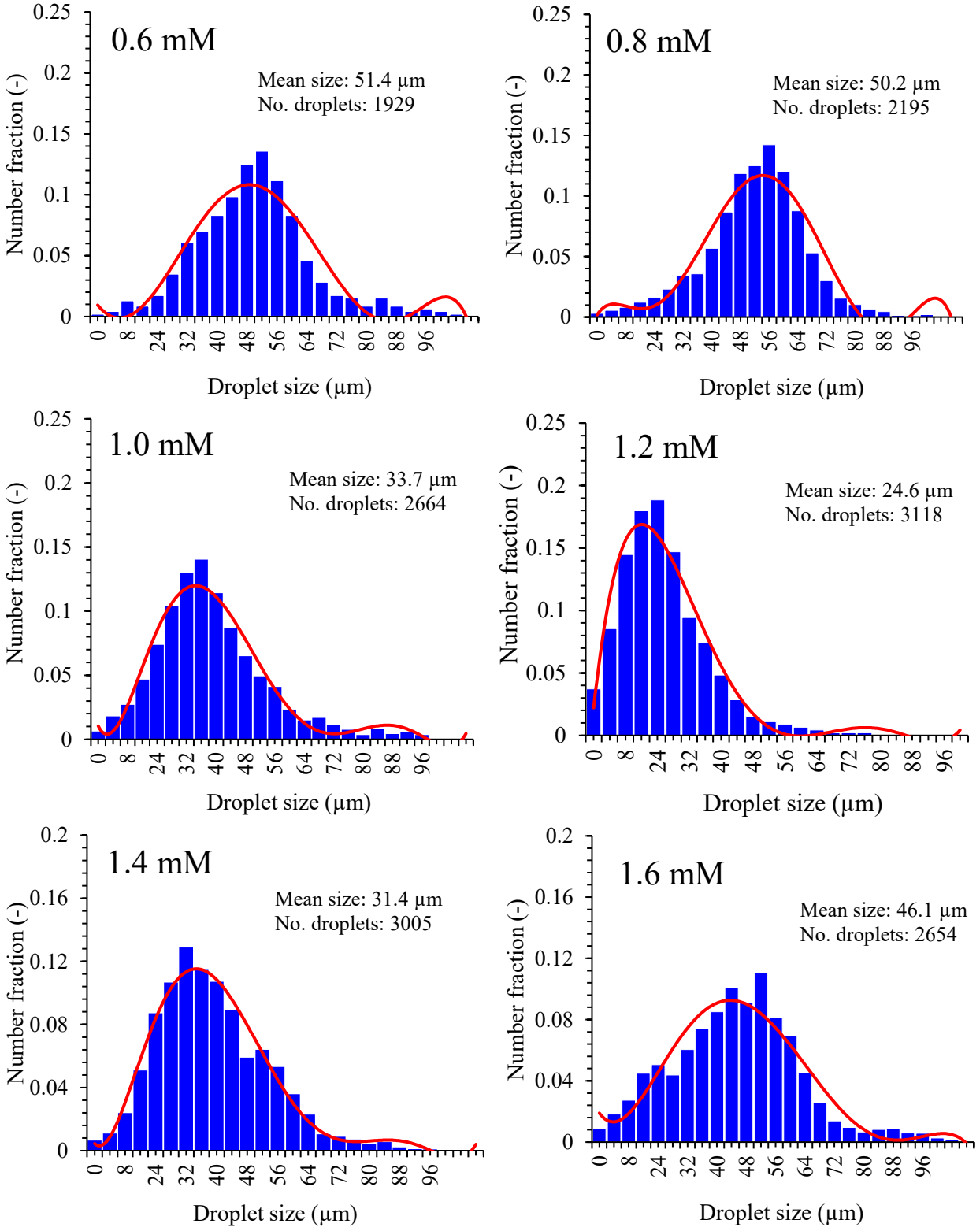

Figure 9. The droplet size distribution of the DE prepared at different Tween 80 concentrations [The W1/O volume ratio was 8:1, while Ca^{2+} and CO_3^{2-} concentrations were 1.2 and 0.8 M, respectively].

3.2. Droplet size distribution of DE after filtration

Figure 10 shows the optical micrographs and droplet size distribution of the DE system after filtration by the POP-based membrane. The Ca^{2+} concentration was 1.2 M, while the W1/O volume ratio was fixed at 6:1. The concentrations of Span 80 and Tween 80 were also fixed to be 1.2 mM. The micrograph obtained from the DE after filtration clearly showed that the size range of the droplets significantly reduced to below ~40 μm with a mean size of 3.7 μm, which showed a 91.9% decrease in the mean droplet size as compared to the DE before filtration (Fig. 4).

A significant reduction in the population of micron-sized droplets captured by the filtrated sample indicates the proposed membrane can successfully control the mean size and droplet size distribution of DE to achieve better droplet size uniformity. A good performance of the proposed membrane can be attributed to the particle size heterogeneity of the PUMA structure, creating a dense multilayer of adsorbed particles, which acts as a barrier against droplet coalescence and passing of large droplets.

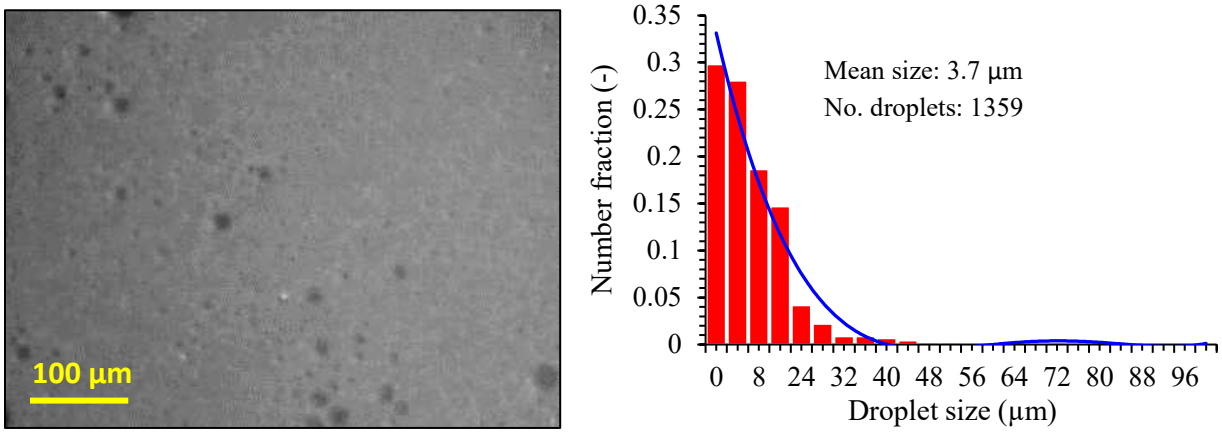

Figure 10. The optical micrographs and corresponding droplet size distribution after filtration by membrane [Ca^{2+} concentration: 1.2 M, W1/O volume ratio: 8:1, and concentrations of Span 80 and Tween 80: 1.2 mM].

3.3. Evaluation of membrane performance

Figure 11 shows the permeate flux and filtration efficiency (%) of the POP-based membrane for the DE prepared at different W1/O volume ratios under optimal conditions. The proposed membrane showed a minimum permeate flux and filtration efficiency (%) to remove oil droplets at low W1/O volume ratios (2:1 and 4:1). This reduction may be attributed to the creation of a denser filter cake formed by the smaller oil droplets on the membrane surface. It is, however, essential to emphasize that the enhancement of the electric field positively influences flux, regardless of the droplet size. Additionally, a reduction in the permeate flux and filtration efficiency (%) of the oily feed solutions was attributed to the attractive force between the membrane surface and oil droplets.

An increase in the W1/O volume ratio from 6:1 to 12:1 led to an increase in the permeate flux and filtration efficiency (%). A maximum permeate flux and filtration efficiency (%) was observed at a W1/O volume ratio of 8:1. The electrostatic repulsion between the membrane surface and the DE system can improve the filtration efficiency (%) of the POP-based membrane towards emulsified oil separation. Additionally, the uniform distribution of droplets at a W1/O volume ratio of 8:1 led to an improvement in the emulsion permeability by reducing the resistance to emulsion flow across the membrane surface. The presence of the membrane was able to prevent the passing of the large droplets and the passing of fine droplets (below 40 μm). This result confirmed that the highly porous structure caused by hierarchical hollow fibers and partial hydrophilic/high oleophobic characteristics of POP particles acts as a molecular sieve site that is able to sieve out large oil droplets caused by oil-oil coalescence and effectively enhance oil permeability. However, the coalescence of nano-sized oil droplets within the hollow fiber structure of the POP-based membrane led to a reduction in its permeability. A minor decrease in the permeate flux and

filtration efficiency (%) of the proposed membrane at a high W1/O volume ratio (12:1) was attributed to a slight increase in the droplet size in the primary W1/O emulsion (Fig. 7).

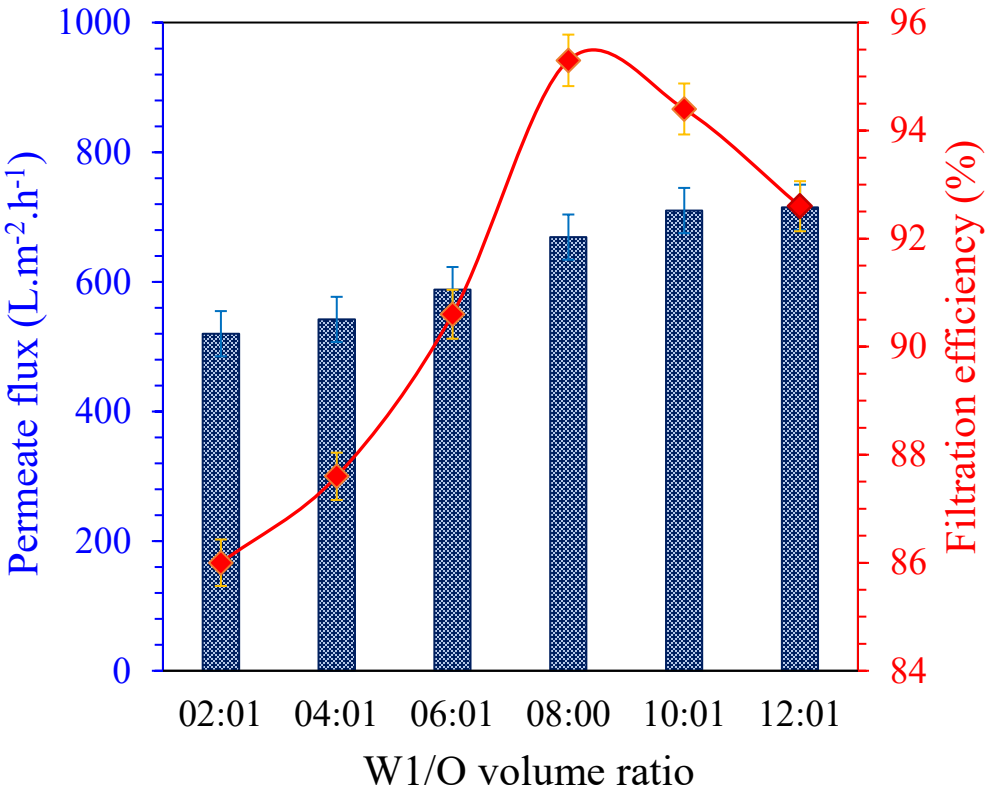

Figure 11. The permeate flux and filtration efficiency (%) of the POP-based membrane for DE system prepared at different W1/O volume ratios under optimum conditions.

Figure 12 shows the fouling resistance evaluation of the POP-based membrane as-prepared in this study. The membrane performance was examined in the feed emulsions at different W1/O volume ratios after four cycles. The results indicated that the proposed membrane has a good fouling resistance, which was influenced by its partial hydrophilic and high oleophobic property of the proposed membrane. On the one hand, the presence of hydroxyl groups in the POP structure led to the form of strong hydrogen bonds with free water droplets, achieving partial hydrophilicity properties. In other hand, the rough surface morphology of proposed membrane led to a reduce in

the oil adhesion, and reinforcing the membrane's oleophobic property, as reported in the literature (Hegab et al. 2024).

The fouling resistance of the POP-based membrane improved with an increase in the W1/O volume ratio of feed emulsion (Fig. 12). At low W1/O volume ratios (less than 8:1), the coalescence of oil droplets on the surface of membrane led a reduction in the fouling resistance of membrane by alleviating filter cake accumulation. At high W1/O volume ratios (more than 8:1), the water droplets accumulate on the membrane surface until a liquid-barrier film with a critical size is reached, and the shear force impedes phase detachment. The results indicated that, even in extended operation of oil-in-water emulsion filtration, the POP-based membrane exhibited stable performance, retaining over 81% of its initial flux even after four cycles. This result indicates the flux stability of the proposed membrane and its ability to control the occurrence of fouling even after extended use (Fig. 12).

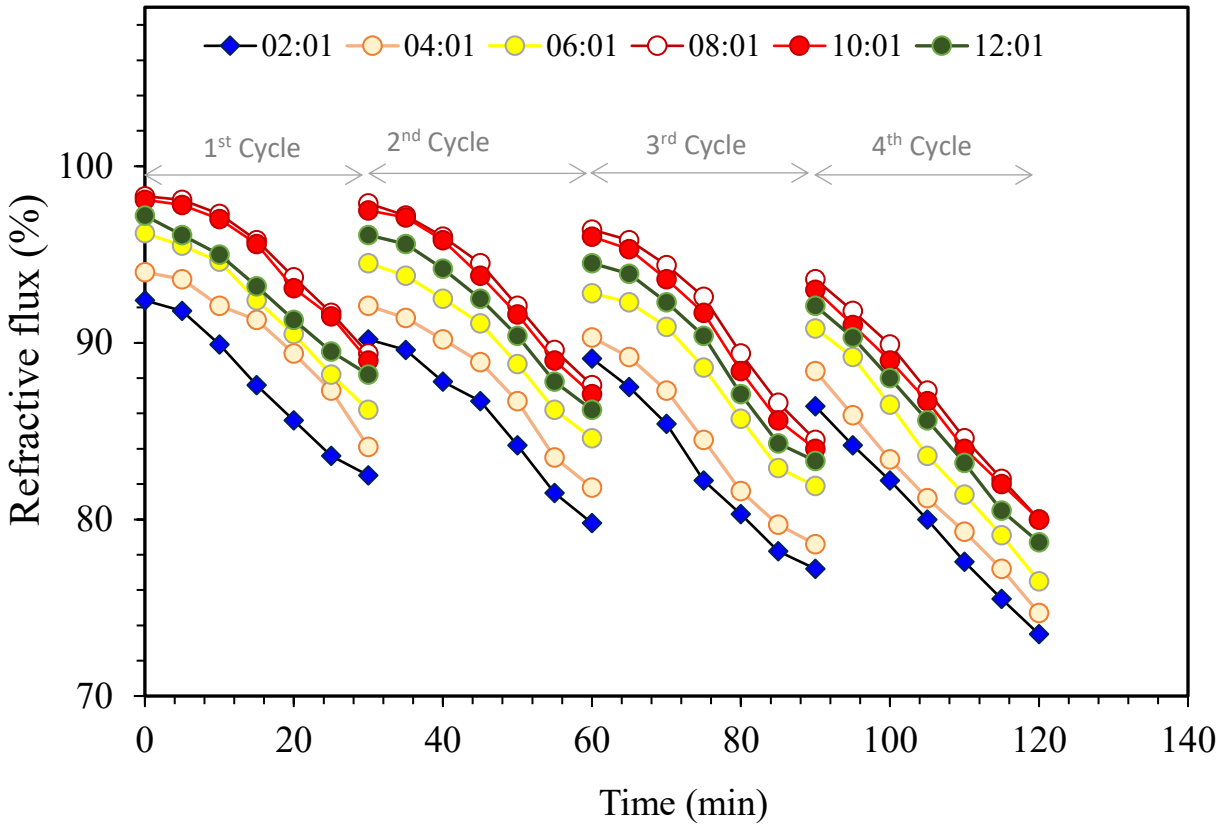

Figure 12. The fouling resistance evaluation of POP-based membrane used in this study [The results were reported in the feed solutions at different W1/O volume ratios after four cycles].

3.4. Characterization of PCC NPs

Figure 13 shows the characterization of the PCC NPs prepared at optimum conditions, including (a) FE-SEM image and corresponding particle size distribution, (b) TEM image, and (c) element analysis. The FE-SEM image of the PCC NPs showed an ellipsoidal geometry with a size distribution ranging from 40 to 100 nm (Fig. 13a). The mean particle size was determined by measuring the size of randomly chosen particles of 61 nm. The FE-SEM image showed that the NPs have a strong tendency to form the agglomerated structures caused by the self-assembly of NPs through the interparticle forces [17]. The TEM image showed the PCC NPs with a mean particle diameter of 72 nm. The rhombohedral calcite crystals of the PCC NPs were revealed from

the TEM micrograph (Fig. 18b). The existence of calcium, carbon, and oxygen was confirmed by EDX analysis (Fig. 18c).

According to EDX analysis, the purity of the nano PCC sample is reported to be about 96%, of which the share of the main transition metals (mercury, lead, cadmium, and arsenic) is about 0.2% by weight of the total sample. The highest number of impurities is related to the three elements: silica, iron, and magnesium. Among the mentioned elements, the highest share of impurities is magnesium, with a value of 71.2%, which is often left behind due to the high formation rate of magnesium chloride in competition with calcium chloride in the purification process of sugar syrup waste. Adjusting the pH conditions can affect the final percentage of the final product (Hanifa et al. 2025). The absence of other organic impurities indicates that the membrane microemulsion process does not cause any elemental contamination in the final sample.

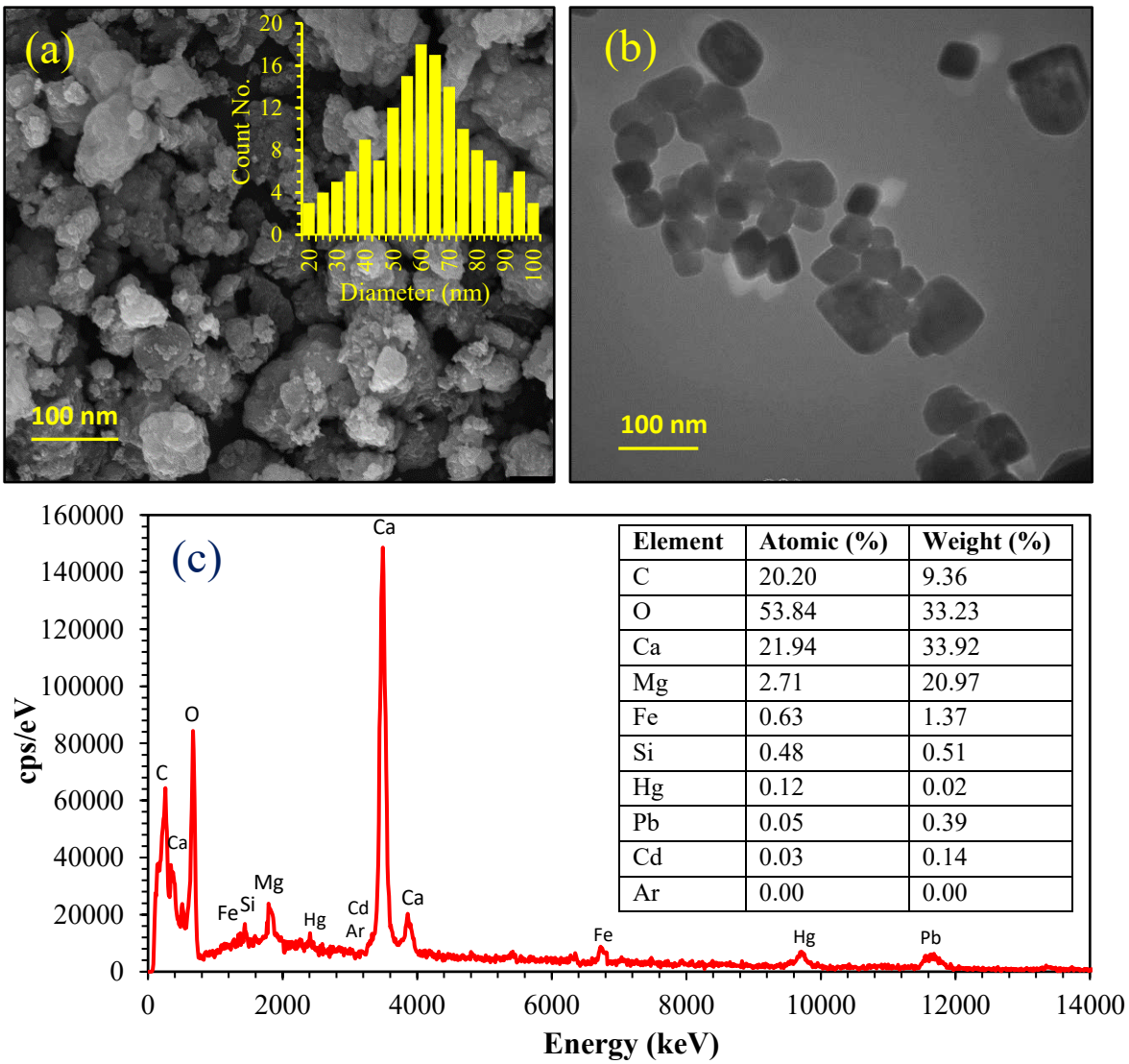

Element	Atomic (%)	Weight (%)
C	20.20	9.36
O	53.84	33.23
Ca	21.94	33.92
Mg	2.71	20.97
Fe	0.63	1.37
Si	0.48	0.51
Hg	0.12	0.02
Pb	0.05	0.39
Cd	0.03	0.14
Ar	0.00	0.00

Figure 13. Characterization of as-prepared PCC NPs: (a) FE-SEM image and particle size distribution, (b) TEM image, and (c) element analysis.

Conclusions

In summary, the size-selective synthesis of precipitated calcium carbonate nanoparticles (PCC NPs) from industrial calcium-rich waste through the liquid-liquid Solvay method was studied through the membrane emulsification method in a bench-scale unit. The effect of the volume ratio of internal aqueous phase to organic phase (W1/O) volume ratio and concentrations of Ca^{2+} as well as surfactants (Span 80 and Tween 80) on the droplet size distribution of the double emulsion (DE)

system were studied before and after membrane emulsification. A novel porous organic polymer (POP)-based membrane consisting of polyurethane-melamine/polyether(sulfone) was developed to obtain a homogeneous droplet size distribution of DE system. The results indicated that the W1/O volume ratio contributed the highest effect on the results to attain a stable DE. An increase in the W1/O volume ratio led to a significant decrease in droplet size, where a narrow droplet size distribution was obtained at a W1/O ratio of 10:1. An increase in Ca^{2+} concentration led to an increase in the mean size of droplets, caused by droplet coalescence phenomena. A well-controlled manner of DE was achieved by attaining the lowest mean particle size, and narrow size distribution. An optimum condition, including a W1/O ratio of 8:1 and a Ca^{2+} concentration of 1.2 M, as well as Span 80 and Tween 80 concentrations of 1.2 mM as critical micelle concentration, was obtained based on the results. The maximum permeate flux and maximum filtration efficiency were achieved at the highest W/O volume ratios of 12:1 and 8:1, respectively. The POP-based membrane possesses a refractive flux recovered by 93% in a continuous three-cycle operation without cleaning, as well as self-cleaning properties and suitable reusability. The proposed membrane acts as a size-selective layer to remove large droplets, attributed to its partial hydrophilicity and high oleophobic properties as well as the presence of the grid-like fibrous spindle structures that can form hierarchical nano-channels.

CRediT authorship contribution statement

Alireza Bahramian: Investigation, Visualization, Methodology, Conceptualization, Writing–review & editing.
Mohammad Mahdi Salmanipour: Formal analysis, Resources, Writing–original draft.

Declaration of Competing Interest

The authors declare that they have no known competing financial interests or personal relationships that could have appeared to influence the work reported in this paper.

Acknowledgements

The authors gratefully acknowledge the financial support provided by the Iran National Science Foundation (INSF) under Grant No. 4040583. The author would also like to thank the Research & Development unit of Bahar Powder Technology Company for their technical supports.

References

Akhtar M, Dickinson E, (2007) Whey protein– maltodextrin conjugates as emulsifying agents: an alternative to gum Arabic Food Hydrocoll 21:607-616. https://doi.org/10.1016/j.foodhyd.2005.07.014

Al Nasser W, Shaikh A, Morriss C, Hounslow M, Salman A (2008) Determining kinetics of calcium carbonate precipitation by inline technique. Chem Eng Sci 63:1381-1389. https://doi.org/10.1016/j.ces.2007.07.051

Bahramiana A, Zarei N, Torabi M, Yarie M, Zolfigol MA (2025) Highly efficient oil-water separation system using urea-bearing porous organic polymer: A comparative study on oil removal efficiency of mixtures and emulsions, Colloids Surf A Physicochem Eng Asp 726:137823. https://doi.org/10.1016/j.colsurfa.2025.137823

Biradar S, Ravichandran P, Gopikrishnan R, Goornavar V. Hall JC, Ramesh V, et al. (2011) Calcium carbonate nanoparticles: synthesis, characterization and biocompatibility. J Nanosci Nanotech 11:6868-6874. https://doi.org/10.1166/jnn.2011.4251

Boyjoo Y, Pareek VK, Liu J (2014) Synthesis of micro and nano-sized calcium carbonate particles and their applications. J Mater Chem A 2:14270-14288. https://doi.org/10.1039/C4TA02070G

Buyukkestelli HI, Nehir El S (2021) Enhancing sweetness using double emulsion technology to reduce sugar content in food formulations, IFSET 74:102809. https://doi.org/10.1016/j.ifset.2021.102809

Bukuaghangin O, Neville A, Charpentier TVJ (2015) Scale formation in multiphase conditions, Proceedings of the Oil Field Chemistry Symposium, Gielo.

Casanova H, Higuita LP (2011) Synthesis of calcium carbonate nanoparticles by reactive precipitation using a high-pressure jet homogenizer. Chem Eng J 175:569-578. https://doi.org/10.1016/j.cej.2011.09.051

Cox S, Sandall A, Smith L, Rossi M, Whelan K (2020) Food additive emulsifiers: a review of their role in foods, legislation and classifications, presence in food supply, dietary exposure, and safety assessment. Nut Rev 79:726-741. https://doi.org/10.1093/nutrit/nuaa038

Chouaibi M, Rezig L, Lakoud A, Boussaid A, Hassouna M, Ferrari G, Hamdi S (2019) Exploring potential new galactomannan source of Retama reatam seeds for food, cosmetic and pharmaceuticals: Characterization and physical, emulsifying and antidiabetic properties, Int J Biol Macromol 124:1167-1176. https://doi.org/10.1016/j.ijbiomac.2018.12.007

Czaplicka N and Konopacka-Łyskawa D (2020) Utilization of gaseous carbon dioxide and industrial Ca-Rich waste for calcium carbonate precipitation: A Review, Energies 13:6239. https://doi.org/10.3390/en13236239

da Silva M, Sad Cristina MS, Filgueiras PR, Eustáquio Castro VR & Robson Alves P (2026) Influence of carbon dioxide and nitrogen gases on W/O emulsion stability: a comparison between Brazilian post-salt and pre-salt oils, Braz J Chem Eng. https://doi.org/10.1007/s43153-026-00691-3

De Hert SC, Rodgers TL (2017) On the effect of dispersed phase viscosity and mean residence time on the droplet size distribution for high-shear mixers. Chem Eng Sci 172:423-433. https://doi.org/10.1016/j.ces.2017.07.002

Dhodduraj K, Narisetty V, Nabavi SA, Parra Saldivar R, Coulon F, Agrawal D, Maity SK, Balan V, Kumar V, (2026) Beets beyond sugar: Potential and limitations of sugar beet pulp as a feedstock for biorefineries, Ind Crops Prod 240:122559. https://doi.org/10.1016/j.indcrop.2025.122559

Fadia P, Tyagi S, Bhagat S, Nair A, Panchal P, Dave H, Dang S, Singh S (2021) Calcium carbonate nano- and microparticles: synthesis methods and biological applications, 3 Biotech 11:457. https://doi.org/10.1007/s13205-02102995-2

Ferdowsi A, Kikhavani T & Ashrafizadeh SN (2025) Enhancement in performance of the PVC/nanoclay mixed matrix nanofiltration membrane, Braz J Chem Eng 42:1183–1195. https://doi.org/10.1007/s43153-024-00485-5

Florence AT, Whitehill D (1981) Some features of breakdown in water-in-oil-in-water multiple emulsions. J Colloid Interface Sci 79:243-256. https://doi.org/10.1016/0021-9797(81)90066-7

Gehrmann S, Bunjes H, (2017) Preparation of nanoemulsions by premix membrane emulsification: which parameters have a significant influence on the resulting particle size? J Pharm Sci 106:2068–2076. https://doi.org/10.1016/j.xphs.2017.04.066

Ghasemi H, Darjani S, Mazloomi H, Mozaffari S (2020) Preparation of stable multiple emulsions using food-grade emulsifiers: evaluating the effects of emulsifier concentration, W/O phase ratio, and emulsification process. SN Appl Sci 2:2002. https://doi.org/10.1007/s42452-020-03879-5

Guo X, Li X, Chan L, Huang W, & Chen T (2021) Edible $CaCO_3$ nanoparticles stabilized Pickering emulsion as calcium- fortifed formulation, Nanobiotechnol 19:67. https://doi.org/10.1186/s12951-021-00807-6

Gupta R (2004) Synthesis of precipitated calcium carbonate nanoparticles using modified emulsion membranes (Master's thesis). https://repository.gatech.edu/server/api/core/bitstreams/93854e9d-e1da-4f1b-9de5-8230af72c8cb/content

Hanifa M, Sharma U, Thapliyal PC & Singh LP (2025) Effects of temperature, pH and calcium-to-carbonate ratio on the calcium carbonate polymorphs, Discov Civ Eng 2:1-20. https://doi.org/10.1007/s44290-025-00291-z

Hailan SM, Ponnamma D, & Krupa I (2021) Separation of oil/water mixtures by modified melamine and polyurethane foams: A Review, Polymer 13:4142. https://doi.org/10.3390/polym13234142

Hegab HM, Elmekawy A, Aubry C, Kallem P, Wadi VS, W Hasan Sh, (2024) 3D hierarchical aquaporin-like nanoporous graphene membrane with engineered tripartite nanochannels for efficient oil/water separation. npj Clean Water 7:1-11. https://doi.org/10.1038/s41545-024-00303-y

Jin Zh, Yu Ch, Wang R, Wei W, Jing Y & Wang Q (2022) Preparation of precipitated calcium carbonate using wollastonite and CO_2 from industrial exhaust, Braz J Chem Eng 39:661–669. https://doi.org/10.1007/s43153-021-00200-8

Kaewnoo S, Wongniramaikul W, Boonkanon Ch, Taweekarn T, Kleangklao B, Limwongsakorn S, Phawachalotorn Ch, Aga DS, Choodum A (2026) Effective recovery of phosphate from wastewater using biodegradable calcium-rich shell wastes composite macroporous cryogel,

Colloids Surf A Physicochem Eng Asp 729:138920. https://doi.org/10.1016/j.colsurfa.2024.133857

Keogh W, Neville A, Huggan M, Eroini V, Olsen JH, Nielsen FM, Baraka-Lokmane S, Bourdelet E, Ellingsen JA, Bache O, Charpentier T (2017) Deposition of inorganic carbonate, sulfate, and sulfide scales on antifouling surfaces in multiphase flow, Energ Fuels 31:11838-11851, https://doi.org/10.1021/acs.energyfuels.7b02165

Kotsuki K, Obata S, Saiki K (2016) Self-aligned growth of organic semiconductor single crystals by electric field, Langmuir 32:644-649. https://doi.org/10.1021/acs.langmuir.5b03975

Krishna Pai R, and Pillai S (2008) Nanoparticles of amorphous calcium carbonate by miniemulsion: synthesis and mechanism, Cryst Eng Comm 10:865-872. https://doi.org/10.1039/b717057b

Kumar A, Kaur R, Kumar V, Kumar S, Gehlot R, Aggarwal P (2022) New insights into water-in-oil-in-water (W/O/W) double emulsions: Properties, fabrication, instability mechanism, and food applications, Trends Food Sci Technol 128:22-37. https://doi.org/10.1016/j.tifs.2022.07.016

Kumar V, Chaudhary P, Ghosh S, Khanam Sh (2025) A review of double emulsions: Microfluidic preparation and CFD simulation, Sustain Chem Climate Action 6:100063. https://doi.org/10.1016/j.scca.2025.100063

Leister N, Karbstein HP (2020) Evaluating the stability of double emulsions- a review of the measurement techniques for the systematic investigation of instability mechanisms. Colloids Interfaces 4:8. https://doi.org/10.3390/COLLOIDS4010008

Leong TSH, Zhou M, Kukan N, Ashokkumar M, Martin GJO (2017) Preparation of water-in-oil-in-water emulsions by low frequency ultrasound using skim milk and sunflower oil, Food Hydrocoll 63:685-695. https://doi.org/10.1016/j.foodhyd.2016.10.017

Li YX, Gong SJ, Guan X, Jiang H, Tao SN, Yang C, Ngai T, Li YX, Gong SJ, Jiang H, Tao SN, Yang C, Guan X, Ngai T (2021) One-step preparation of all-natural Pickering double emulsions stabilized by oppositely charged biopolymer particles. Adv Mater Interfaces 8:2101568. https://doi.org/10.1002/ADMI.202101568

Liu L, Ou G, Xu L, Ogiwara N, Uchida S, Yang H, Sakai Y, (2024) Simultaneous productions of high-purity calcium carbonate and amorphous nanosized silica-rich gel from waste concrete powder by alkaline treatment and carbonation, J Env Manage 372:123319. https://doi.org/10.1016/j.jenvman.2024.123319

Liu J, Liu S, Zhong L, Li Z, Chen X, & Yuan S (2025) Advances of emulsification during the lifetime development of heavy oil reservoirs. Adv Colloid Interface Sci 340:103445. https://doi.org/10.1016/j.cis.2025.103445

Maghamian N, Goli M, Najarian A (2021) Ultrasound-assisted preparation of double nano-emulsions loaded with glycyrrhizic acid in the internal aqueous phase and skim milk as the external aqueous phase, LWT 141:110850. https://doi.org/10.1016/j.lwt.2021.110850

Marinova KG, Alargova RG, Denkonv ND, Velev OD, Petsev DN, Ivanov IB, Borwankar RP (1996) Charging of oil-water interfaces due to spontaneous adsorption of hydroxyl ions, Langmuir 12:2045-2051. https://doi.org/10.1021/la950928i

Matos M, Guti´errez G, Iglesias O, Coca J, Pazos C (2015) Enhancing encapsulation efficiency of food-grade double emulsions containing resveratrol or vitamin B12 by membrane emulsification, J Food Eng 166:212–220. https://doi.org/10.1016/j.jfoodeng.2015.06.002

Márquez AL, Medrano A, Panizzolo LA, Wagner JR (2010) Effect of calcium salts and surfactant concentration on the stability of water-in-oil (w/o) emulsions prepared with polyglycerol polyricinoleate. J Colloid Interface Sci 341:101-108. https://doi.org/10.1016/j.jcis.2009.09.020

Pei Y, Chen P, Li Sh, Wang J (2023) Producing amorphous calcium carbonate using waste Ca-rich solution generated through the bio-leaching of slag, Sustain Chem Pharm 36:101333. https://doi.org/10.1016/j.scp.2023.101333

Sharma S, Simsek H (2020) Sugar beet industry process wastewater treatment using electrochemical methods and optimization of parameters using response surface methodology, Chemosphere, 238:124669. https://doi.org/10.1016/j.chemosphere.2019.124669

Stawski TM, Roncal-Herrero T, Fernandez-Martinez A, Matamoros-Veloza A, Kröger R, Benning LG (2018) ‘‘on demand” triggered crystallization of $CaCO_3$ from solute precursor species stabilized by the water-in-oil microemulsion, Phys Chem Chem Phys 20:13825-13835, https://doi.org/10.1039/ c8cp00540k

Pal R (2008) Viscosity models for multiple emulsions. Food Hydrocoll 22:428-438. https://doi.org/10.1016/J.FOODHYD.2006.12.012

Rauscher F, Veit P, Sundmacher K (2005) Analysis of a technical-grade w/o-microemulsion and its application for the precipitation of calcium carbonate nanoparticles, Colloids Surf A Physicochem Eng Asp 254:183-191. https://doi.org/10.1016/j.colsurfa.2004.11.034

Reichhardt C, & Parsek MR (2019) Confocal laser scanning microscopy for analysis of pseudomonas aeruginosa biofilm architecture and matrix localization. Front Microbiol 10:677. https://doi.org/10.3389/FMICB.2019.00677/BIBTEX

Somani RS, Patel KS, Mehta AR, Jasra RV (2006) Examination of the polymorphs and particle size of calcium carbonate precipitated using still effluent (*i.e.*, $CaCl_2$ + NaCl solution) of soda ash manufacturing process. Ind Eng Chem Res 45:5223-5230.https://doi.org/10.1021/ie0513447

Tang X, Zhou L, Liao J, Zhou Y, Zhou J (2025) In situ immobilization of CO_2 from coal-to-hydrogen off-gas to co-produce calcium carbonate nanoparticles using a modified membrane reactor, Surf Interfaces 62:106163. https://doi.org/10.1016/j.surfin.2025.106163

von Smoluchowski M (1921) Handbuch der Elektrizität und des Magnetismus, Band. II, Barth-Verlag, Leipzig, pp. 366-427.

Yeh Sh-L, Koshani R, Sheikhi A (2023) Colloidal aspects of calcium carbonate scaling in water-in-oil emulsions: A fundamental study using droplet-based microfluidics, J Colloid and Interface Sci 633:536-545. https://doi.org/10.1016/j.jcis.2022.11.066

Yegya Raman AK, Aichele CP (2020) Influence of non-ionic surfactant addition on the stability and rheology of particle-stabilized emulsions, Colloids Surf A Physicochem Eng Asp 585 124084. https://doi.org/10.1016/j.colsurfa.2019.124084

Wang Q, Gao C, Yang L, Zhou P, Sun D (2026) Generation of double emulsion droplets with controllable intra- and extra-droplet trehalose concentration in a six-way microfluidic chip, Colloids Surf A Physicochem Eng Asp 728:138742. https://doi.org/10.1016/j.colsurfa.2025.138742

Zhang JL, Huang XF, Xiong YJ, Zheng WW, Liu WQ, He MF, Li LX, Liu J, Lu LJ, Peng KM (2022) Spider silk bioinspired superhydrophilic nanofibrous membrane for efficient oil/water separation of nanoemulsions, Sep Purif Technol 280:119824. https://doi.org/10.1016/j.seppur.2021.119824

Zhang R, Huo J-H, Peng Zh-G, Luo W-J, Feng Q, Wang J-X, Zhang J (2016) Study on the interaction of $CaCO_3$ nanoparticles and surfactant in emulsion phase transition and its molecular dynamics simulation, Colloids Surf A Physicochem Eng Asp 511:105–112. http://dx.doi.org/10.1016/j.colsurfa.2016.09.034

Supplementary Files

This is a list of supplementary files associated with this preprint. Click to download.

- GAFinal.pptx